Concentration effects on turbulence in dilute polymer solutions far from walls

Alexandre de Chaumont Quitry and Nicholas T. Ouellette

Phys. Rev. E **93**, 063116 — Published 24 June 2016

DOI: 10.1103/PhysRevE.93.063116

Concentration effects on turbulence in dilute polymer solutions far from walls

Alexandre de Chaumont Quitry[1] and Nicholas T. Ouellette[2, 1, *]

[1] *Department of Mechanical Engineering & Materials Science, Yale University, New Haven, Connecticut 06520, USA*

[2] *Department of Civil and Environmental Engineering, Stanford University, Stanford, California 94305, USA*

We report measurements of the modification of turbulence far from any walls by small concentrations of long-chain polymers. We consider a range of statistical properties of the flow, including Eulerian and Lagrangian velocity structure functions, Eulerian acceleration correlation functions, and the relative dispersion of particle pairs. In all cases, we find that the polymer concentration has a strong effect on the extent to which the statistical properties are changed compared to their values in pure water. These effects can be captured by the recently proposed energy flux balance model (when suitably extended into the time domain for Lagrangian statistics). However, unlike previous measurements, which found that the concentration effect could be completely scaled out, we consistently find that our data collapses onto two different master curves, one for small concentration and one for larger concentration. We suggest that the difference between the two may be related to the onset of interactions among polymer chains, which is likely to be more easily observed at the small Weissenberg numbers we consider here.

PACS numbers: 47.27.Gs, 47.57.Ng, 47.50.-d

I. INTRODUCTION

Both the material and flow properties of fluids can be changed by adding mesoscale structure. Such complex fluids display a vast range of behaviors, from shear thinning or thickening to viscoelasticity and more. In the context of turbulent flows, it has been known since the pioneering work of Toms [1] that additives can dramatically reduce the skin-friction drag in turbulent wall-bounded flows [2]. Toms worked with long-chain polymers, and we focus on polymers here; however, macroscopically similar turbulent drag reduction has also been demonstrated for other kinds of additives such as surfactants [3], rigid fibers [4], or microbubbles [5, 6]. Rather remarkably, this drag reduction can be observed with only a tiny amount of additive (on the order of parts per million by weight), well below the limit where material properties such as the shear viscosity are modified significantly from their Newtonian values.

The essential physics underlying skin-friction drag reduction appears to be a thickening of the buffer layer and an associated modification of the near-wall turbulent structures, which in turn disrupts the turbulence regeneration cycle in the boundary layer [2, 7]. However, experimental observations over the past few decades have demonstrated that the statistical properties of isotropic turbulence far from any boundaries can also be modified by polymers [8–17]. Thus, the presence of a wall and the turbulent structures it produces are not a necessary condition for turbulence modification, although it remains possible that the mechanisms responsible for the flow modifications may be qualitatively different in the wall-bounded and isotropic cases.

Qualitatively, the addition of polymers to the flow has been observed to lead to an effective attenuation of the usual Richardson–Kolmogorov energy cascade at small scales. The signature of this attenuation is usually a reduction in the mean-field energy dissipation rate per unit mass ϵ at a length scale near the lower end of the cascade but still within the inertial range [16, 17]. In some previous experiments, the turbulence was driven via boundary-layer interactions, such as in grid-generated turbulence [8, 12], Taylor–Couette turbulence [9], or in a counter-rotating-disc von Kármán swirling flow with smooth discs [10]. In these cases, the reduction in the energy dissipation may partially be attributable to a decrease in the energy *injection* into the turbulence via standard skin-friction drag reduction. However, experiments that drove the flow inertially and therefore roughly maintained the energy injection rate when polymers were added [11] have also seen changes to the effective small-scale energy dissipation [14, 16, 17]. Numerical simulations of isotropic turbulence in polymer solutions, where the polymers are modeled by a continuum field that couples to the turbulence, have also found modifications of the energy cascade, where polymers can extract turbulent kinetic energy from the flow and at least partially dissipate it directly [18].

Here, we focus on the role played by the polymer concentration in modifying the statistics of a turbulent counter-rotating disc flow. We consider a wide range of turbulence statistics, including Eulerian and Lagrangian velocity structure functions, the spatial correlation functions of acceleration, and the relative dispersion of particle pairs. In all cases, we find that the recently proposed elastic energy flux balance model [17] captures the essential effect of the polymer concentration, when appropriately extended into the time domain. However, unlike in previous work that found that this model could collapse

* nto@stanford.edu

data from a broad range of polymer concentrations and flow conditions onto a single master curve [17], our results show *two* clearly distinguishable families of curves. Although a complete understanding of this behavior remains elusive, we argue that the different behavior we see may be due to the onset of possible interactions between polymer molecules as they are stretched by the turbulent velocity gradients.

We begin below by outlining the essential aspects of the interplay between polymers and turbulence in Sec. II. We then describe our experimental apparatus and data acquisition methods in Sec. III. Our results for Eulerian statistics are presented in Sec. IV, followed by measurements of Lagrangian statistics in Sec. V. Finally, we discuss the implications of our measurements in Sec. VI.

II. BACKGROUND

Long-chain polymer molecules can be thought of as entropic springs. In equilibrium, they coil into tightly packed conformations, maximizing their entropy. Under applied stresses, however, they can be stretched out into elongated configurations, at the cost of a stored elastic energy. Once the applied stress is removed, they will tend to re-coil on a characteristic relaxation time scale τ_p. For polymers suspended in a fluid, the ratio of τ_p to the inverse of the shear rate, known as the Weissenberg number Wi, will determine whether the polymers tend to be elongated (when Wi > 1 and shearing occurs more quickly than relaxation) or coiled (when Wi < 1). In turbulence, the Weissenberg number is typically defined as Wi $= \tau_p/\tau_\eta$, where τ_η is the Kolmogorov time scale, since the inverse of the shear rate is of order τ_η.

Various aspects of this picture of polymers as springs have been used to suggest mechanisms for how polymers affect turbulence, and in particular to estimate at what scale the energy cascade is likely to be modified. Lumley [19] focused on the temporal behavior of the polymers and chose the relaxation time τ_p to be the most important parameter characterizing the polymers. Applying Kolmogorov-style arguments, he then argued that the cascade should be modified beginning at a length scale $r^* = (\epsilon\tau_p^3)^{1/2}$, at which the local scale-dependent Weissenberg number exceeds unity and the polymers will be stretched by the action of the turbulent eddies faster than they can relax. This argument, however, leaves no room for the effects of varying polymer concentration, and its predictions have not been verified by experiments outside the boundary layer [16, 17].

A different picture based on the polymer energetics was proposed by Tabor & De Gennes [20, 21]. They argued that it is not the change in polymer conformation per se that modifies the turbulence; rather, it is the the fact that stretched polymer molecules store elastic energy that is the more fundamental mechanism for flow modification. The only source for this elastic energy is the kinetic energy of the turbulent fluctuations, which must therefore be damped by the addition of polymers. Indeed, numerical simulations have demonstrated that polymers can effectively siphon kinetic energy from the turbulence [18]. Thus, although Tabor & De Gennes agreed with Lumley [19] that the polymers are stretched by the flow beginning at a scale r^*, they introduced a new (smaller) length scale r^{**} to characterize the onset of the polymer back-reaction on the flow. r^{**} is defined to be the length scale at which the elastic energy stored in the polymer molecules balances the scale-dependent turbulent kinetic energy, determined by Kolmogorov-style arguments. Specifically, r^{**} is defined implicitly by

$$\frac{1}{2}c_p k_B T \left(\frac{r^*}{r^{**}}\right)^{5n/2} = \frac{1}{2}\rho u_{r^{**}}^2 = \frac{1}{2}\rho\left(\epsilon_T r^{**}\right)^{2/3} \qquad (1)$$

The left-hand side of this equation is the elastic energy (per unit mass) stored by the polymers; c_p is the number of polymer molecules per unit volume, k_B is Boltzmann's constant, and T is the temperature. Together, $c_p k_B T$ is an estimate of the net elastic modulus of the polymer phase. n is an exponent that depends on the characteristics of local flow deformation that stretches; $n = 1$ corresponds to the case of two stretching directions and one compressive, as is typically found in turbulent flows [17]. The right-hand side of this equation is the turbulent kinetic energy (per unit mass) at the scale r^{**}. ρ is the mass density of the fluid, and standard Kolmogorov scaling is used to re-express the scale-dependent velocity in terms of the length scale r^{**} and the rate of energy transfer per unit mass through the inertial range ϵ_T. We note that this notation is somewhat non-standard; typically, ϵ with no subscript is used. In non-Newtonian turbulence, however, it is necessary to distinguish the rate of energy injection into the turbulent cascade, which we denote by ϵ_I, the rate of energy transfer through the inertial range ϵ_T, and the rate of energy dissipation by viscosity ϵ_D [16, 17]. In Newtonian turbulence, $\epsilon_I = \epsilon_T = \epsilon_D = \epsilon$, by conservation of energy. In the polymer case, however, these equalities need not hold, as (particularly in the Tabor & De Gennes framework) the polymers can provide a non-viscous mechanism for drawing energy out of the turbulent cascade.

This elastic energy balance model has the appealing feature that r^{**} is concentration dependent, since higher polymer concentration means more polymer molecules, and more molecules can store more energy. This model also introduces the possibility of a critical concentration: if r^{**} falls below the Kolmogorov length scale η, the polymers will no longer affect the turbulence. However, the assumptions underlying this model have been criticized [22], and, more seriously, it is not internally self-consistent [17]. It assumes that the polymers are stretched at r^*, but only affect the flow at r^{**}; but at the same time they are assumed to affect the flow because polymer stretching siphons kinetic energy from the cascade, which should occur whenever they are stretched.

A resolution of this conundrum that keeps some of the appealing features of the elastic energy balance model

was recently proposed and tested experimentally by Xi *et al.* [17]. They modified the Tabor & De Gennes picture by arguing that the relevant quantity that should be balanced to determine the scale at which polymers affect the flow is not the energy itself, but rather (as this is a dynamically evolving system) the *rate* of energy transfer. The rate of elastic energy transfer can be estimated by dividing the Tabor & De Gennes estimate of the elastic energy stored in the polymers by the polymer relaxation time τ_p, since τ_p is the time scale on which the polymers will release this stored energy, while the rate of turbulent kinetic energy transfer is simply given by ϵ_T. Balancing these quantities predicts that the polymers should affect the cascade at a scale

$$r_\epsilon = A \left(\frac{k_B T}{\rho} \right)^{2/(5n)} c_p^{2/(5n)} \epsilon_T^{(1/2)-(2/(5n))} \tau_p^{(3/2)-(2/(5n))}, \tag{2}$$

where A is an unknown scaling constant and n is the same exponent that appears in equation 1. By analyzing data from an experiment similar to the one described here, Xi *et al.* [17] determined that $n \approx 1$ and $A \approx 100$, and were able to collapse the data from experiments over a range of Reynolds numbers and polymer concentrations by re-scaling by r_ϵ. For our purposes, the key prediction of this energy flux balance model is that, for fixed turbulence parameters and polymer properties, we would expect lengths in the cascade to be re-scaled by a factor of $c_p^{2/5}$. The energy flux balance model also predicts that r_ϵ should vary with the energy transfer rate ϵ_T, which may (weakly) change with the addition of polymers to the flow (see, for example, fig. 1(b) below). With $n = 1$, however, r_ϵ scales only as $\epsilon_T^{1/10}$, and so we neglect it here and only consider the (stronger) scaling with polymer concentration.

III. APPARATUS AND DATA ACQUISITION

A. von Kármán Swirling Flow

We generated turbulence in a closed plexiglass cylindrical tank measuring 89 cm in height and 58 cm in diameter by counter-rotating two impellers aligned axially along the centerline of the cylinder. The impellers themselves have a diameter of 44 cm, so that they occupy a large fraction of the cross-sectional area of the tank. The distance between the impellers is 50 cm, so that the actively driven volume of the flow has a nearly unit aspect ratio.

As discussed above, we seek a driving mechanism that is as inertial as possible, rather than one that couples to the fluid though boundary-layer interactions. Each of the impellers is therefore fitted with 5 cm straight vanes rather than being smooth. The impellers are driven by independent AC motors that are mechanically geared down to provide sufficient torque to drive the fluid without undue rotation speed. As the injected kinetic energy is dissipated by viscous action, heat in generated in the working fluid. To prevent the water temperature from rising over time, we run temperature-controlled water through double-spiral channels in the aluminum top and bottom plates of the apparatus. Because the turbulence mixes efficiently, this boundary cooling is sufficient to maintain a roughly uniform temperature throughout the apparatus with no mean gradients. We monitor the temperature via four thermocouples placed inside the apparatus; measurements from these thermocouples show that the temperature is constant in time and uniform in space to within less than 0.1 °C.

For the data presented here, the rotation rate of each impeller was controlled to be 0.23 Hz. By measuring the Eulerian velocity structure functions (see below), we find that in pure water this rotation rate corresponds to a Taylor-microscale Reynolds number of $R_\lambda = 420$. The integral length scale L is measured to be 14.2 cm by estimating the energy dissipation rate ϵ from the structure functions for several different rotation rates and assuming that $\epsilon = u'^3/L$, where u' is the turbulence intensity, as is typically done in these kinds of flows [23]. The Kolmogorov length scale η is 124 μm, and the Kolmogorov time scale τ_η is 15.2 ms, as determined from their definitions.

B. Particle Tracking

To measure the flow, we use three-dimensional Lagrangian particle tracking [24]. We seed the fluid with 30 μm polystyrene microspheres that contain a fluorescent dye that absorbs in the green and fluoresces in the red. We excite the particles with a Q-switched Nd:YAG laser running at a pulse rate of 10 kHz and with an average power of 45 W. The motion of the particles is then recorded by three Photron Fastcam SA5 cameras at a rate of 2000 frames per second at a resolution of 1024×1024 pixels. This frame rate corresponds to approximately 30 images per τ_η at this Reynolds number. The three cameras have an angular separation of 45° in the horizontal plane; the central camera is positioned 30° out of plane to improve the depth resolution of the system. Using the method of Tsai [25], we calibrate the imaging system by assuming a pinhole model for each camera, and fix the model parameters by imaging a grid of evenly spaced dots with a known spacing. We can then use this model to reconstruct the three-dimensional positions of the tracer particles using standard stereo-imaging techniques [24]. For the data presented here, we image a volume with a linear dimension of 2.3 cm in the center of the apparatus.

We use a three-frame best-estimate predictive tracking algorithm to combine the time-resolved three-dimensional particle positions into trajectories [24]. Accurate velocities and accelerations are then computed along the trajectories by convolving the tracks with a smoothing and differentiating kernel [26]. Lagrangian

statistics can be naturally computed from the raw trajectories; and since we measure many particles at each time step, Eulerian statistics can also be obtained from the contemporaneous particle measurements.

C. Polymer Solutions

For the results presented here, we used a high-molecular-weight (18×10^6 a.m.u.) polyacrylamide (Poly-Sciences 18522) as our flow additive, at concentrations ϕ ranging from 1 to 20 parts per million (ppm) by weight. We note that c_p defined above is the number density of polymer chains, whereas ϕ is the weight/weight concentration; one is easily obtainable from the other, given knowledge of the solvent, and they scale linearly with one another for any given polymer. The concentrations we consider here are low enough (an order of magnitude below the overlap concentration, for example) that the change in shear viscosity due to the polymers is negligible and that the longest relaxation times of the solutions should be independent of concentration [27].

For this polymer, the radius of gyration R_g at equilibrium is roughly 0.5 μm, and the fully stretched length is about 75 μm. The relaxation time τ_p (calculated using the Zimm model) is 43 ms, giving us a Weissenberg number (based on the Kolmogorov time scale) of Wi = 2.8.

To prepare the polymer solutions, we dissolve the appropriate mass of dry polymer in 2 liters of deionized water by gentle stirring over a 12-hour period to create a high-concentration stock solution. We then gravity-feed this stock solution into the turbulence apparatus, avoiding any mechanical degradation that may occur if we were to use a pump. To ensure that the polymers are distributed homogeneously in the apparatus, we spin the impellers at a low rotation rate (0.14 Hz) for periods of up to a few hours before acquiring data. This procedure has been shown in previous, similar experiments to lead to robust, repeatable results [15].

Mechanical degradation and chain scission is always a concern when studying polymers in turbulence: if the turbulent strain rate is large enough to stretch polymers appreciably, fluctuations in the strain rate may be large enough to break the chains. If the chains begin to break, the effective polymer concentration will decrease. To check for degradation, we monitored the acceleration variance as measured from the tracer particles as a function of time for each of our data runs, as this variance has been shown to be quite sensitive to the polymer concentration [15]. For each concentration, we acquired data over a period of about 30 hours. Although there are certainly fluctuations in the acceleration variance, we observed that the mean value of the variance did not change with time over the course of the experiment. We also note that we used this test to determine the fastest impeller rotation rate, and therefore largest Reynolds number, we could safely study without polymer degradation; at higher rotation rates, we *did* observe a change in the acceleration variance over time.

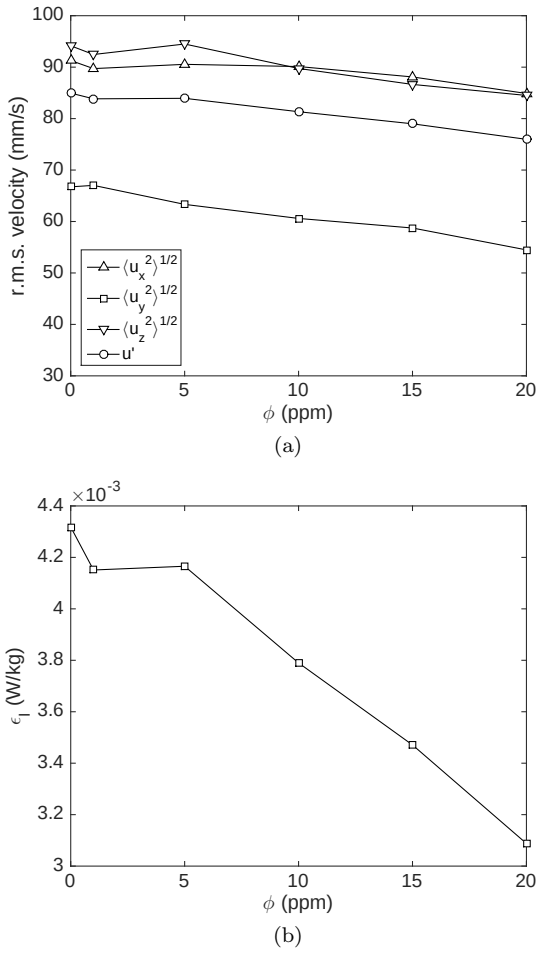

FIG. 1. (a) Root-mean-square (r.m.s.) velocity as a function of the polymer concentration ϕ. Data are shown for the three independent directions in the experiment (y is the axial direction) and for the turbulence intensity u'. (b) Estimate of the energy injection rate $\epsilon_I = u'^3/L$ as a function of ϕ.

IV. EULERIAN STATISTICS

A. Large-scale Flow

As described above, we drive the flow with baffled discs to minimize the impact of drag reduction at the forcing element [11]. Nevertheless, some modification of the large-scale flow is likely unavoidable, since we are not injecting energy and momentum into the flow via a volumetric body force. To estimate how much the large scales of the flow were modified after the polymers were added, we measured the root-mean-square (r.m.s.) velocity as a function of polymer concentration ϕ, as shown in figure 1(a). We show both the three velocity components (with $\langle u_x^2\rangle^{1/2}$ and $\langle u_z^2\rangle^{1/2}$ in the radial plane of the apparatus and $\langle u_y^2\rangle^{1/2}$ in the axial direction) as well as

the turbulence intensity $u' = \left[(1/3)\langle u_x^2 + u_y^2 + u_z^2\rangle\right]^{1/2}$. The trend for all the velocity components is similar, decreasing weakly with concentration. By $\phi = 20$ ppm, the r.m.s. velocities are about 10% lower than their measured values in pure water.

Although the decrease in velocity is fairly small, it may have a somewhat larger effect on the energy injected into the cascade. The energy injection rate ϵ_I is of order u'^3/L, where L is the integral length scale; thus, a small change in u' leads to a larger change in ϵ_I. We show this estimate of ϵ_I as a function of concentration in figure 1(b). ϵ_I does indeed fall off more sharply with concentration, particularly for $\phi > 5$ ppm. Thus, some of the decrease in the measured energy dissipation that we will describe below should be attributed to a decrease in energy injection.

B. Velocity Structure Functions

In addition to a potential global damping of turbulence via a weakening of the energy injection, polymers are also widely thought to selectively smooth the velocity field at small scales, weakening some of the intense velocity gradients that are responsible for a significant part of the turbulent dissipation [10]. This effect is qualitatively apparent by simple observation of the trajectories of tracer particles in Newtonian turbulence and in water with a small concentration of polymers, as shown in figure 2. However, to quantify the selective damping of various turbulent scales, we must turn to a more precise statistical measure.

The Eulerian velocity structure functions, defined as the statistical moments of spatial velocity increments, are standard tools to characterize the turbulent energy cascade, and, as in a sense coarse-grained velocity gradients, are sensitive to the spatial structure of the flow field in the inertial range. Here, we focus on the second-order structure functions. Given values of the velocity field at positions $\mathbf{x}$ and $\mathbf{y}$, we define the velocity increment to be $\delta\mathbf{u}(\mathbf{x},\mathbf{y}) = \mathbf{u}(\mathbf{y}) - \mathbf{u}(\mathbf{x})$. In homogeneous turbulence, $\delta\mathbf{u}$ depends only on the distance between the two points $\mathbf{r} = \mathbf{y} - \mathbf{x}$. The second-order Eulerian velocity structure function tensor is then defined to be $D_{ij}(\mathbf{r}) = \langle \delta u_i(\mathbf{r}) \delta u_j(\mathbf{r})\rangle$. In isotropic turbulence, this tensor can be completely characterized by the two scalar functions $D_{LL}(r)$ (the longitudinal structure function, where the velocities are taken to be parallel to $\mathbf{r}$) and $D_{NN}(r)$ (the transverse structure function, where the velocities are perpendicular to $\mathbf{r}$). Here, we show only data for the transverse structure function D_{NN}; in experiments, it is typically better resolved, since in three dimensions there are two independent measurements of D_{NN} per pair of velocities.

In isotropic turbulence, one expects that

$$D_{NN}(r) = \frac{4}{3} C_2 (\epsilon_T r)^{2/3} \tag{3}$$

for $\eta \ll r \ll L$, where η is the Kolmogorov length scale and L is the integral length scale. C_2 is expected to be a universal constant, with a measured value of 2.13 [28]. Although there may be some intermittency corrections to the scaling exponents, at second order they are expected to be very small [29]. Thus, the compensated structure function

$$\left[\frac{3}{4}\frac{D_{NN}(r)}{C_2 r^{2/3}}\right]^{3/2} = \epsilon_T \tag{4}$$

can be used to estimate the energy transfer rate through the inertial range in Newtonian turbulence, since in the inertial range it should be constant and equal to ϵ_T. Based on previous results [16, 17], we do not expect the scaling in eq. 3 to change in polymer solutions. Thus, we use the compensated structure functions here to study the details of the statistics of turbulence in polymer solutions with the baseline scaling removed.

In figure 3(a), we show these compensated transverse structure functions both for pure water and for polymer data at varying concentrations. The polymer concentration ϕ clearly has a significant influence on the statistical properties of the flow. As has been seen before [16, 17], as the concentration goes up, two effects are apparent: the compensated structure functions reach their plateau values at larger length scales, and the plateau values are different from the water data. These effects are particularly apparent in our data for $\phi \geq 10$ ppm. We note that the plateau value for the $\phi = 1$ ppm and $\phi = 5$ ppm data are actually slightly larger than for the pure water case; they are likely, however, to be within the expected uncertainty in this measurement, which can be large [30].

The horizontal axis in figure 3(a) is scaled by η^w, the Kolmogorov length scale computed for pure water at this impeller rotation rate. However, this scaling is expected to be modified in the presence of polymers; Xi *et al.* [17], for example, observed a collapse of data for different polymer concentrations when scaling by r_ϵ as derived from their energy flux balance model. As discussed above, that model predicts that lengths should re-scale by a factor of $\phi^{2/5}$. Thus, in figure 3(b), we scale the horizontal axis by $\eta^w \phi^{2/5}$. Like Xi *et al.* [17], we do observe a collapse of the data; however, unlike Xi *et al.* [17], our data collapses onto two distinctly different curves, one for $\phi \leq 5$ ppm and a second for $\phi \geq 10$ ppm. Our results are thus more similar to Ouellette *et al.* [16], who reported a possible critical concentration of $\phi \approx 7$ ppm. Xi *et al.* [17] ascribed the absence of a critical concentration in their data to a re-design of the experimental apparatus, and in particular to the lack of vanes on the sidewalls of the their von Kármán flow (which were present in the experiments of Ouellette *et al.* [16]). However, in our apparatus we also do not have vanes, and yet still see what may be a critical concentration.

It should also be noted that the critical concentration described by Ouellette *et al.* [16] separated concentrations for which the structure functions measured in the polymer data reached a plateau value of ϵ_T (as mea-

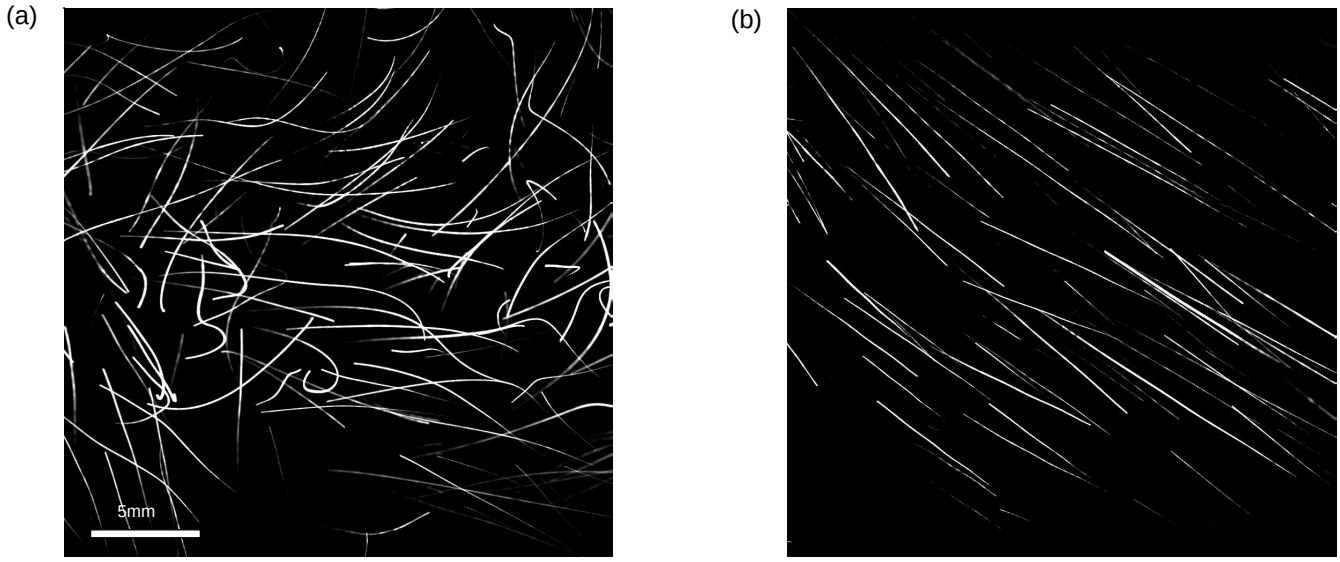

FIG. 2. Long-exposure (50 ms $\approx 3.3.\tau_\eta^w$) images of the trajectories of tracer particles as seen by the center camera in (a) pure water and (b) a 10 ppm polymer solution. The trajectories are noticeably smoother and more spatially coherent in the polymer solution.

sured from pure water) from those that did not. At first glance, we see similar behavior here. However, as noted above in figure 1(b), we do see some decrease in ϵ_I, the large-scale energy injection rate, for larger concentrations. When we scale the compensated structure functions by the measured, concentration-dependent ϵ_I, as shown in figure 3(c), the peak values for all concentrations are similar, although the two distinct families of collapsed curves are still evident. Therefore, the potential critical concentration we find may be distinct from that observed by Ouellette *et al.* [16].

An understanding of the factors responsible for the differences between our results, those of Ouellette *et al.* [16], and those of Xi *et al.* [17] remains elusive. All three experiments were performed in flows with a similar geometry, the same polymer, and the same measurement tools; but different results were obtained. Each data set is also internally consistent; as we show below, for example, different statistics calculated from our data all give consistent results. The difference between the three experiments therefore suggests that there may be some as-yet-unknown additional parameters necessary for characterizing turbulence in dilute polymer solutions.

C. Acceleration Correlations

Turbulence in polymer solutions is often qualitatively described as being more spatially smooth than Newtonian turbulence at the same Reynolds number. This notion can be made somewhat more concrete by studying, for example, spatial correlation functions. The velocity correlations, however, are not necessarily a good choice for this purpose. They fall off (by definition) on length scales comparable to the integral length scale, which is difficult to capture in any experiment that seeks to resolve the small scales of the flow and where we cannot make use of Taylor's frozen-flow hypothesis due to the finite number of camera pixels, and they can additionally suffer seriously from finite-volume biases. In addition, the velocity correlations are not local in scale, and so the Kolmogorov hypotheses cannot be used to predict their scaling [31].

Some of these issues can be mitigated, however, by considering the correlations of the acceleration. As predicted by Obukhov & Yaglom [32], these correlations both decay over shorter length scales and have a Kolmogorov scaling form in the inertial range that agrees well with experimental measurements [33]. We define the acceleration correlation tensor as

$$R_{ij}(\mathbf{r}) = \langle a_i(\mathbf{x}) a_j(\mathbf{x}+\mathbf{r}) \rangle, \tag{5}$$

where $a_i(\mathbf{x})$ is the i^{th} component of the full material acceleration; that is,

$$a_i = \frac{\partial u_i}{\partial t} + \mathbf{u} \cdot \nabla u_i. \tag{6}$$

Also, note that strictly speaking R_{ij} is a covariance rather than a correlation, since we are not normalizing by the acceleration variance. Just as for the velocity structure function, assuming statistical isotropy allows one to

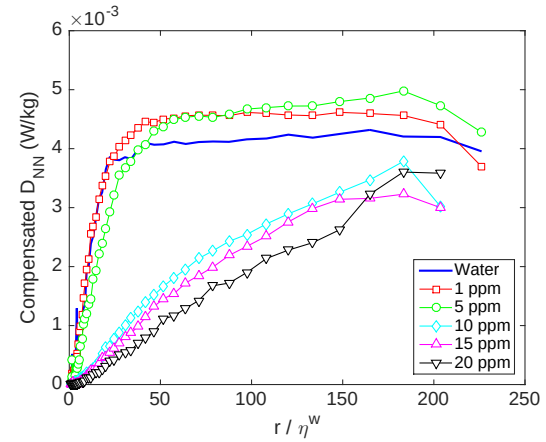

(a)

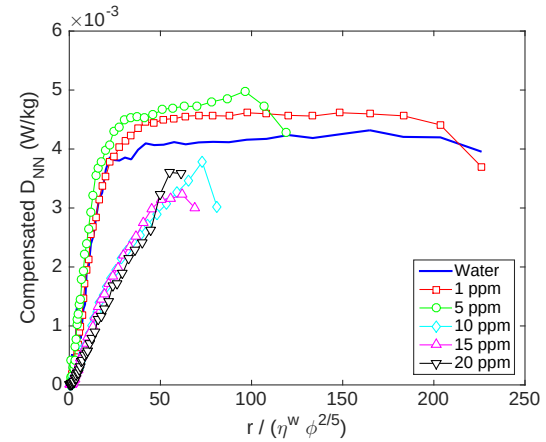

(b)

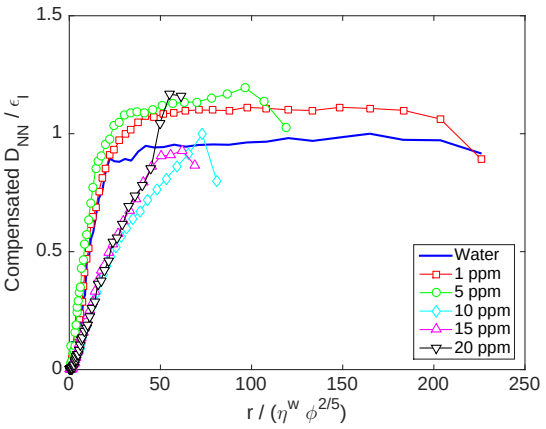

(c)

FIG. 3. (color online) (a) Compensated transverse structure function D_{NN} (see equation 4) as a function of r/η^w, where η^w is the Kolmogorov scale measured from the water data. (b) The same data as in panel (a), but with length rescaled by a factor of $\phi^{2/5}$, as expected from the energy flux balance model. (c) The same data as in panel (b), but with the vertical axis rescaled by the measured concentration-dependent values of ϵ_I (see figure 1(b)).

decompose R_{ij} into longitudinal and transverse components R_{LL} and R_{NN}, respectively; and also like for the structure functions, we report here only measurements of R_{NN}.

Obukhov & Yaglom [32] showed that, under some simplifying assumptions, R_{NN} can be related to the velocity structure function D_{NN} (via the pressure structure functions), and thereby predicted that

$$R_{NN}(r) = \frac{2}{3} C_2^2 \epsilon_T^{5/3} r^{-2/3} \tag{7}$$

in the inertial range [33]. As with the velocity structure functions, we can compensate the acceleration correlation as

$$\left[\frac{3}{2} \frac{r^{2/3} R_{NN}(r)}{C_2^2} \right]^{3/5} = \epsilon_T \tag{8}$$

to estimate ϵ_T and to make a detailed comparison of the effects of polymer concentration.

In figure 4, we show our measurements of R_{NN}, compensated according to equation 8, for pure water and for varying polymer concentrations. In figure 4(a), we scale the separation r by η^w, while in figure 4(b) we also include the expected concentration dependence of $\phi^{2/5}$. Although there results are less dramatic than for the velocity structure functions, similar behavior is seen: once we include the concentration scaling, we see the data collapse onto two master curves, with high-concentration data behaving differently from low-concentration data. We also note that the plateau value, which according to equation 8 should be ϵ_T, is much lower than the estimate from the velocity structure functions, and is additionally nearly the same for all values of ϕ without re-scaling by ϵ_I as in figure 3(c). The most likely cause of this discrepancy is under-resolution of the acceleration, since it is very difficult to measure the enormous fluctuations of acceleration accurately [23], particularly with the relatively low frame rate we have used here. However, we also note the possibility that, since the acceleration is a very small-scale quantity, the plateau value of the acceleration correlations may be related more strongly to the viscous energy dissipation rate ϵ_D rather than the energy transfer rate ϵ_T, even though the inertial-range scaling prediction for the velocity structure function is used in deriving equation 8. Obukhov & Yaglom [32], of course, made no distinction between ϵ_D and ϵ_T, since they are the same in Newtonian turbulence.

V. LAGRANGIAN STATISTICS

A. Velocity Structure Functions

Just as in the Eulerian context, velocity structures have played a central role in characterizing the Lagrangian properties of turbulence. In the Lagrangian

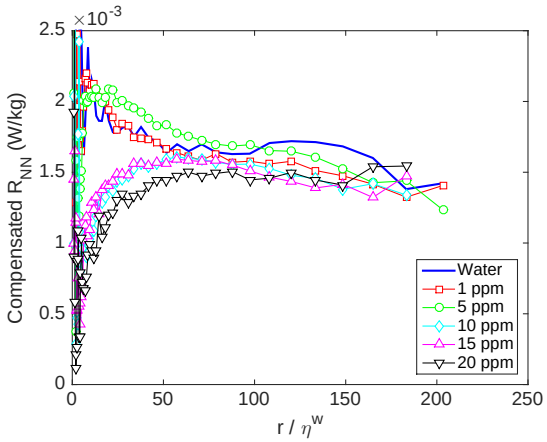

(a)

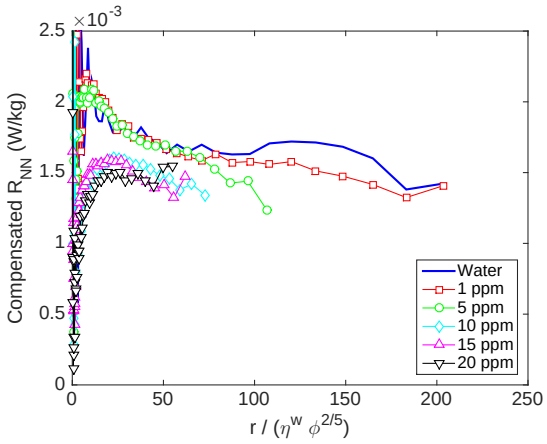

(b)

FIG. 4. (color online) (a) The transverse acceleration correlation function R_{NN}, compensated by the inertial range scale prediction as in equation 8, with lengths scaled by η^w. (b) The same data as in panel (a), but with lengths rescaled by $\phi^{2/5}$.

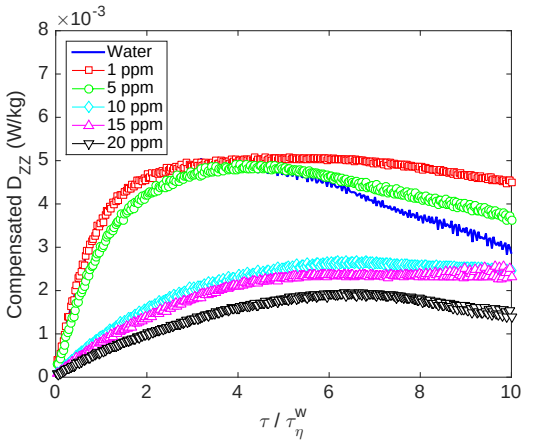

(a)

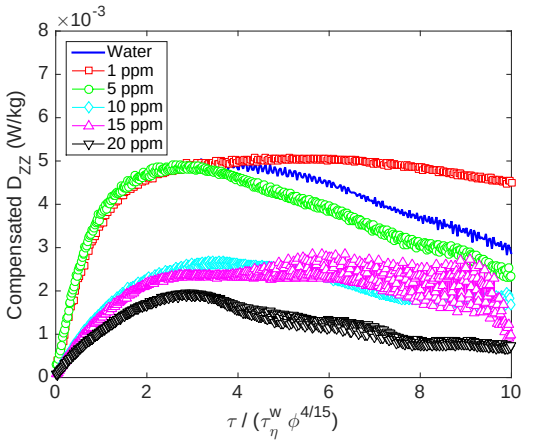

(b)

FIG. 5. (color online) (a) The second-order Lagrangian structure function D_{ZZ} (z is in the radial plane of the experiment) compensated by $C_0\tau$, with time scaled by τ_η^w, the Kolmogorov time scale computed for the water data. (b) The same data as in panel (a), but with time rescaled by a factor of $\phi^{4/15}$.

framework, the structure functions are still the statistical moments of the velocity increments $\delta\mathbf{u}$; in contrast to the Eulerian case, however, the increments are now taken along Lagrangian trajectories and are explicit functions of time only. In particular, the second-order Lagrangian structure function is given by $D_{ij}^L = \langle \delta u_i(\tau)\delta u_j(\tau)\rangle$, where τ is the time lag separating the two velocity measurements along a single trajectory. In isotropic turbulence, $D_{ij}^L(\tau)$ must be an isotropic tensor and therefore proportional to the identity tensor δ_{ij}, since τ is a scalar.

Applying Kolmogorov theory, one expects that

$$D_{ij}^L(\tau) = C_0\epsilon_T\tau\delta_{ij} \tag{9}$$

in the Lagrangian inertial range (that is, for $\tau_\eta \ll \tau \ll T_L$, where τ_η is the Kolmogorov time scale and T_L is the integral time scale). C_0 is again a constant that is expected to be universal, although there is less consensus on its value that on the corresponding Eulerian constant C_2. In a similar flow at the Reynolds number considered, its value was measured to be $C_0 \approx 6$ in the radial plane [34], and that is the value we use here in defining the compensated structure function. We also note that, as is typical in von Kármán flows, the effective value C_0, as well as the velocity fluctuations themselves (see figure 1(a)), tend to be smaller in the axial direction (y, in our convention). Here, we therefore only report one the radial components of D_{ij}^L, D_{zz}^L.

In figure 5(a), we plot $D_{zz}^L(\tau)$ compensated by $C_0\tau$ for water and for varying polymer concentrations, with time scaled by τ_η^w, the Kolmogorov scale for the water data. Several features are immediately evident. First, the scaling range is very short even for the water data (if indeed the Lagrangian structure functions scale at all [35]). Additionally, as with our Eulerian results, there is a clear concentration effect: both the peak value of the structure functions and the position of this peak shift

with ϕ.

The energy flux balance model gives us a way to capture the variation of spatial, Eulerian statistics with ϕ. However, it is not obvious how to use the flux-balance model to capture *temporal* re-scaling. The elastic energy stored by the polymers is explicitly due to their stretching, and is therefore connected to length scales, not time scales. The only natural time scale in the model is the polymer relaxation time τ_p, but τ_p is not concentration-dependent.

Instead, we here propose a simple physical picture to estimate how times should re-scale in the presence of polymers. In the energy flux balance model, the key physics involves the stretching of the polymers by turbulent eddies of scale r_ϵ, which is determined by balancing the rate of turbulent energy transfer through an eddy of scale r_ϵ and the rate at which polymers release the stored elastic energy when they are stretched to a length r_ϵ. So, to define a time scale from this picture, we use the Kolmogorov estimate of the lifetime of an eddy of size r_ϵ, namely

$$t_\epsilon = \left(\frac{r_\epsilon^2}{\epsilon_T}\right)^{1/3}. \tag{10}$$

Inserting r_ϵ from equation 2, we therefore expect that times should rescale with concentration by a factor of $\phi^{4/15}$. We note that t_ϵ is also the Kolmogorov estimate for the strain rate at the scale r_ϵ; thus, this argument is equivalent to requiring that the scale-local strain rate be sufficient to stretch the polymers.

To test this scaling prediction, in figure 5(b), we plot the compensated Lagrangian structure function with the time axis scaled by an additional factor of $\phi^{4/15}$. Although the collapse is not as clean as it was for the Eulerian structure functions (figure 3(b)), the position of the peak does approximately overlap for the different concentrations. And, just as with the Eulerian structure functions, we find two classes of behavior, with qualitative differences between $\phi \leq 5$ ppm and $\phi \geq 10$ ppm.

B. Relative Dispersion

The Lagrangian description of fluid flow is intimately connected to transport and mixing. In turbulence, one must typically distinguish between the advection of material away from a fixed source and the growth and spreading of an initialized localized cloud of material [31]. The former problem is dominated by the temporal velocity correlations and can be modeled as a (turbulent) diffusion process [36]; but the latter shows nontrivial turbulence scaling. As first described by Richardson [37], the simplest parameterization of the spread of a cloud is the separation of two initially nearby fluid elements, termed relative dispersion [38, 39].

In the inertial range, the mean-squared separation $r(t)$ is expected to show two distinct scalings [31]:

$$\langle (r(t)-r_0)^2 \rangle = \begin{cases} \frac{11}{3} C_2 (\epsilon_T r_0)^{2/3} t^2, & \tau_\eta \ll t \ll t_0 \\ g \epsilon_T t^3, & t_0 \ll t \ll T_L \end{cases}, \tag{11}$$

where r_0 is the initial separation of the pair. For short times $t \ll t_0 = (r_0^2/\epsilon_T)^{1/3}$ for which r_0 remains an important parameter, the separation scales ballistically in time in the so-called Batchelor regime. In this time range, the pair can be thought of as residing on the same turbulent eddy of scale r_0, and so their statistics are dominated by the difference in velocity across this eddy—and therefore by the Eulerian velocity structure function at scale r_0. This is the origin of the coefficient $(11/3)C_2(\epsilon_T r_0)^{2/3}$, the trace of the second-order Eulerian structure function.

At longer times (but still shorter than the integral time scale T_L) for which the initial separation is forgotten and the eddy the two particles initially belonged to has broken up, the separation should enter the universal Richardson regime; g is known as the Richardson constant. Because the scale separation must be incredibly large to observe two distinct power-law scalings in the inertial range, the Reynolds number must be very high to distinguish these two cases [40]. At our Reynolds number, therefore, we would not expect to see Richardson dispersion even for the water case; however, we do expect robust Batchelor scaling. And, since relative dispersion in the Batchelor scaling regime is dominated by the statistics of the Eulerian structure functions [41], we would expect to observe similar polymer effects as we have shown above.

In figure 6(a), we plot the mean-squared pair dispersion scaled by the Batchelor prediction, so that the curves would plateau at ϵ_T if the Batchelor scaling holds (that is, we plot $\langle (r(t)-r_0)^2 \rangle^{3/2} / \left[(11/3) C_2 r_0^{2/3} t^2\right]$) for initial pair separations lying in the range 10 mm $< r_0 <$ 11 mm. The time axis is scaled by $t_0 = (r_0^2/\epsilon_T)^{1/3}$. As would be expected given the results shown above, there is a strong polymer concentration effect; as ϕ increases, the effective value of ϵ_T appears to decrease. Consistently, the curves begin to deviate from the Batchelor scaling prediction (in the expected way [40, 41]) at later times as ϕ increases.

In figure 6(b) and (c), we attempt to collapse the dispersion data by scaling time and space according to the energy flux balance model; that is, lengths are rescaled by $\phi^{2/5}$ and times by $\phi^{4/15}$. We note that in the Batchelor regime, data must be considered separately for different initial pair separations, as r_0 is an explicit parameter; thus, we must also scale the initial separations by $\phi^{2/5}$. In figure 6(b), we show the compensated dispersion data for initial separations of $r_0 \in [20, 30]\eta^w \phi^{2/5}$, with both axes rescaled to account for concentration effects. Just as we have shown above, the data fall onto two distinct families of curves, one for lower concentrations (and pure water), and one for higher concentrations. The collapse is not quite as clean for the larger concentrations, some of which could be due to the small initial separations: scales of $\sim 20\eta^w$ are only marginally in the inertial range.

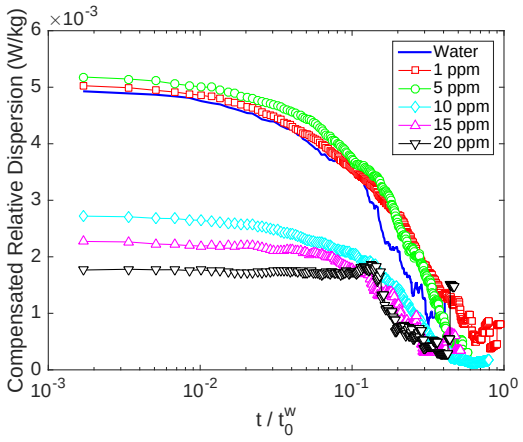

(a)

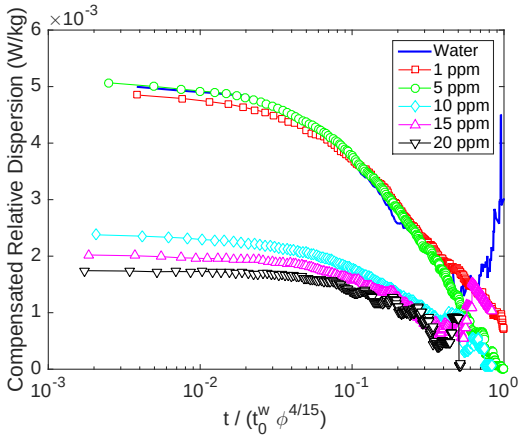

(b)

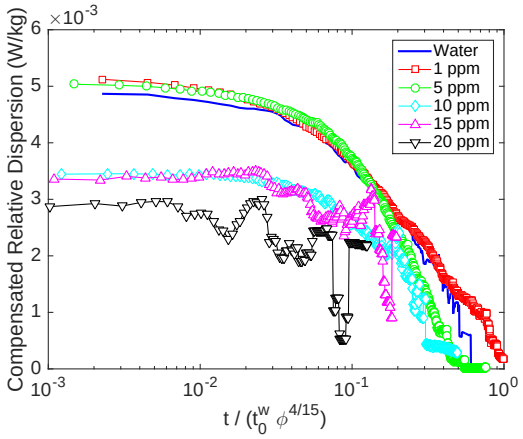

(c)

FIG. 6. (color online) (a) Mean-squared pair separation scaled by the Batchelor prediction (see equation 11 and the text) to obtain ϵ_T, as a function of time scaled by t_0^w, as calculated from the water data alone for initial pair separations $r_0 \in [10, 11]$ mm. (b) Similar data, but with all lengths rescaled by $\phi^{2/5}$ and all times by $\phi^{4/15}$, for initial separations $r_0 \in [20, 30]\eta^w\phi^{2/5}$. (c) Data scaled as in panel (b), but with $r_0 \in [50, 60]\eta^w\phi^{2/5}$.

We therefore also consider larger initial separations with $r_0 \in [50, 60]\eta^w\phi^{2/5}$ in figure 6(c). The trend is very similar, but the data are again somewhat noisy. In this case, the noise is likely statistical; at high concentrations, these initial separations are quite large in physical units, and so not many pairs with these initial separations remain in our measurement volume for long times. For both figure 6(b) and (c), however, we note that the temporal recalling (that is, rescaling the horizontal axis by a factor of $\phi^{4/15}$) appears to work quite well: the curves peel away from the Batchelor prediction at about the same concentration-corrected time scale, at a value that is consistent with earlier experimental findings for pure water [40, 41].

VI. DISCUSSION AND CONCLUSIONS

We have presented here a wide range of turbulence statistics for flow in dilute polymer solutions. Although these metrics include both Eulerian and Langrangian measures, and measure position, velocity, and acceleration, they present a consistent picture. In all cases, the concentration scaling predicted by the energy flux balance model [17] appears to work quite well, even when translated into the time domain. However, unlike what has been seen before in experiments, we also consistently observe two families of curves that independently collapse; one for small concentrations with $\phi \leq 5$ ppm, and one for larger concentrations with $\phi \geq 10$ ppm. This behavior is unexpected, and somewhat mysterious.

A full understanding of the effects we see will require future detailed experimentation and testing; here, however, we offer one possible explanation for the data. The energy flux balance model (and, indeed, most models of turbulence modification by additives) assumes that the polymers are very dilute, and therefore that each polymer chain can be treated as independent. This is expected to be a good approximation at concentrations such as those we consider here. For this polymer, the overlap concentration ϕ^* at which it begins to break down has been estimated to be in the range of 200-250 ppm [42]. However, as the polymers begin to stretch, their effective size grows, and they may begin to interact more than would be expected given their equilibrium size in water. ϕ^* should scale as the inverse cube of the polymer radius of gyration R_g, since it is determined by estimating when the volumes occupied by nearby polymer chains begin to intersect. We can use this scaling and the value of ϕ^* at equilibrium to estimate that if the difference in the two families of curves we see between $\phi = 5$ ppm and $\phi = 10$ ppm were due to the stretched polymers passing out of the dilute regime, we would expect the effective size of the polymers to be about 3 to 4 times larger than their equilibrium radius of gyration R_g.

Measuring the actual extension of the polymer chains in our experiment is not possible. We can, however, estimate the likely mean polymer extension by comparing

our experimental parameters to models. Numerical simulations of bead-spring models of polymer chains in turbulence have suggested that a fairly sharp coil/stretch transition occurs at a Weissenberg number (based on the Kolmogorov scale) of about 3 [43], after which the polymers are nearly fully extended. Here, however, our Weissenberg number is smaller (Wi = 2.8), and may be in the narrow transitional range between fully coiled polymers and fully stretched chains. At this Weissenberg number, the simulations suggest the mean polymer extension should be about 5% of the fully stretched chain length [43]—quite similar to our estimate above. Thus, it is plausible that the qualitative difference between the families of curves we see may be due to the polymers passing out of the dilute regime, given the turbulent dynamics, for our higher concentrations but not our lower concentrations. This argument would also explain why Xi *et al.* [17] did not see the two families of curves we observe here. Nearly all of their data was taken for Weissenberg numbers larger than the coil-stretch transition, and so any effects due to changes in the polymer conformation would be frozen out; from the standpoint of the polymer concentration, their data were all asymptotic. We note that a similar sensitivity to Weissenberg number was found in numerical simulations of homogeneous shear turbulence in polymer solutions by Robert *et al.* [44]. These authors reported a low Weissenberg number regime where the flow was very sensitive to small changes in the polymer effects and a high Weissenberg number regime where it was less so. Although their mechanism may be different, both because the flow had a strong mean shear and because the polymers were represented by a continuum field so that there were no individual polymer chains to interact, the core physics may be similar to what we argue here.

In summary, we conducted measurements of various turbulence statistics, both Eulerian and Lagrangian, in a dilute solution of long-chain polymers at high Reynolds number but moderate Weissenberg number over a range of concentrations. Our results are mostly consistent with the recently proposed energy flux balance model; however, we routinely see a collapse of our data onto two master curves, not one, when the effect of concentration is taken into account. Although a full understanding of this effect is still elusive, we suggest that the transition may be due to the onset of interactions between the individual polymer chains. These results argue that the detailed effects of polymer concentration on turbulence are still not fully understood.

ACKNOWLEDGMENTS

This work was supported by the US National Science Foundation under grant no. CBET-1436423. We appreciate helpful conversations with R. Ni, G. Voth, and H. Xu during this work.

[1] B. A. Toms, "Some observations on the flow of linear polymer solutions through straight tubes at large Reynolds numbers," in *Proc. First Intl. Congr. Rheol.* (North-Holland Publishing, Amsterdam, the Netherlands, 1948) pp. 135–141.

[2] C. M. White and M. G. Mungal, "Mechanics and prediction of turbulent drag reduction with polymer additives," Annu. Rev. Fluid Mech. **40**, 235–256 (2008).

[3] J. L. Zakin, B. Lu, and H. W. Bewersdorff, "Surfactant drag reduction," Rev. Chem. Eng. **14**, 253–320 (1998).

[4] J. S. Paschkewitz, Y. Dubief, and E. S. G. Shaqfeh, "The dynamic mechanism for turbulent drag reduction using rigid fibers based onLagrangian conditional statistics," Phys. Fluids **17**, 063102 (2005).

[5] T. H. van den Berg, D. P. M. van Gils, D. P. Lathrop, and D. Lohse, "Bubbly turbulent drag reduction is a boundary layer effect," Phys. Rev. Lett. **98**, 084501 (2007).

[6] S. L. Ceccio, "Friction drag reduction of external flows with bubble and gas injection," Annu. Rev. Fluid Mech. **42**, 183–203 (2010).

[7] I. Procaccia, V. S. L'vov, and R. Benzi, "Colloquium: Theory of drag reduction by polymers in wall-bounded turbulence," Rev. Mod. Phys. **80**, 225–247 (2008).

[8] W. D. McComb, J. Allan, and C. A. Greated, "Effect of polymer additives on the small-scale structure of grid-generated turbulence," Phys. Fluids **20**, 873–879 (1977).

[9] P. Tong, W. I. Goldburg, and J. S. Huang, "Measured effects of polymer additives on turbulent-velocity fluctuations at various length scales," Phys. Rev. A **45**, 7231–7241 (1992).

[10] D. Bonn, Y. Couder, P. H. J. van Dam, and S. Douady, "From small scales to large scales in three-dimensional turbulence: The effect of diluted polymers," Phys. Rev. E **47**, R28–R32 (1993).

[11] O. Cadot, D. Bonn, and S. Douady, "Turbulent drag reduction in a closed flow system: Boundary layer versus bulk effects," Phys. Fluids **10**, 426–436 (1998).

[12] E. van Doorn, C. M. White, and K. R. Sreenivasan, "The decay of grid turbulence in polymer and surfactant solutions," Phys. Fluids **11**, 2387–2393 (1999).

[13] A. Liberzon, M. Guala, B. Lüthi, W. Kinzelbach, and A. Tsinober, "Turbulence in dilute polymer solutions," Phys. Fluids **17**, 031707 (2005).

[14] A. Liberzon, M. Guala, W. Kinzelbach, and A. Tsinober, "On turbulent kinetic energy production and dissipation in dilute polymer solutions," Phys. Fluids **18**, 125101 (2006).

[15] A. M. Crawford, N. Mordant, H. Xu, and E. Bodenschatz, "Fluid acceleration in the bulk of turbulent dilute polymer solutions," New J. Phys. **10**, 123015 (2008).

[16] N. T. Ouellette, H. Xu, and E. Bodenschatz, "Bulk turbulence in dilute polymer solutions," J. Fluid Mech. **629**, 375–385 (2009).

[17] H.-D. Xi, E. Bodenschatz, and H. Xu, "Elastic energy flux by flexible polymers in fluid turbulence," Phys. Rev. Lett. **111**, 024501 (2013).

[18] P. C. Valente, C. B. da Silva, and F. T. Pinho, "The effect of viscoelasticity on the turbulent kinetic energy cascade," J. Fluid Mech. **760**, 39–62 (2014).

[19] J. L. Lumley, "Drag reduction in turbulent flow by polymer additives," J. Polymer Sci. **7**, 263–290 (1973).

[20] M. Tabor and P. G. de Gennes, "A cascade theory of drag reduction," Europhys. Lett. **2**, 519–522 (1986).

[21] P. G. de Gennes, "Towards a scaling theory of drag reduction," Physica A **140**, 9–25 (1986).

[22] G. Ryskin, "Turbulent drag reduction by polymers: a quantitative theory," Phys. Rev. Lett. **59**, 2059–2062 (1987).

[23] G. A. Voth, A. La Porta, A. M. Crawford, J. Alexander, and E. Bodenschatz, "Measurement of particle accelerations in fully developed turbulence," J. Fluid Mech. **469**, 121–160 (2002).

[24] N. T. Ouellette, H. Xu, and E. Bodenschatz, "A quantitative study of three-dimensional Lagrangian particle tracking algorithms," Exp. Fluids **40**, 301–313 (2006).

[25] R. Y. Tsai, "A versatile camera calibration technique for high-accuracy 3D machine vision metrology using off-the-shelf TV cameras and lenses," IEEE J. Robotic. Autom. **RA-3**, 323–344 (1987).

[26] N. Mordant, A. M. Crawford, and E. Bodenschatz, "Experimental Lagrangian probability density function measurement," Physica D **193**, 245–251 (2004).

[27] Y. Liu, Y. Jun, and V. Steinberg, "Concentration dependence of the longest relaxation times of dilute and semi-dilute polymer solutions," J. Rheol. **53**, 1069 (2009).

[28] K. R. Sreenivasan, "On the universality of the Kolmogorov constant," Phys. Fluids **7**, 2778–2784 (1995).

[29] F. Anselmet, Y. Gagne, E. J. Hopfinger, and R. A. Antonia, "High-order velocity structure functions in turbulent shear flows," J. Fluid Mech. **140**, 63–89 (1984).

[30] N. T. Ouellette, H. Xu, and E. Bodenschatz, "Measuring Lagrangian statistics in intense turbulence," in *Springer Handbook of Experimental Fluid Mechanics*, edited by C. Tropea, J. Foss, and A. Yarin (Springer-Verlag, Berlin, 2007) pp. 789–799.

[31] G. K. Batchelor, "The application of the similarity theory of turbulence to atmospheric diffusion," Q. J. R. Meteorol. Soc. **76**, 133–146 (1950).

[32] A. M. Obukhov and A. M. Yaglom, "The microstructure of turbulent flow," Prikl. Mat. Mekh. **15**, 3–26 (1951), English translation as NACA TM 1350, 1953.

[33] H. Xu, N. T. Ouellette, D. Vincenzi, and E. Bodenschatz, "Acceleration correlations and pressure structure functions in high-Reynolds number turbulence," Phys. Rev. Lett. **99**, 204501 (2007).

[34] N. T. Ouellette, H. Xu, M. Bourgoin, and E. Bodenschatz, "Small-scale anisotropy in Lagrangian turbulence," New J. Phys. **8**, 102 (2006).

[35] G. Falkovich, H. Xu, A. Pumir, E. Bodenschatz, L. Biferale, G. Boffetta, A. S. Lanotte, and F. Toschi, "On Lagrangian single-particle statistics," Phys. Fluids **24**, 055102 (2012).

[36] G. I. Taylor, "Diffusion by continuous movements," Proc. Lond. Math. Soc. **20**, 196–212 (1922).

[37] L. F. Richardson, "Atmospheric diffusion shown on a distance-neighbour graph," Proc. R. Soc. Lond. A **110**, 709–737 (1926).

[38] B. Sawford, "Turbulent relative dispersion," Annu. Rev. Fluid Mech. **33**, 289–317 (2001).

[39] J. P. L. C. Salazar and L. R. Collins, "Two-particle dispersion in isotropic turbulent flows," Annu. Rev. Fluid Mech. **41**, 405–432 (2009).

[40] M. Bourgoin, N. T. Ouellette, H. Xu, J. Berg, and E. Bodenschatz, "The role of pair dispersion in turbulent flow," Science **311**, 825–838 (2006).

[41] N. T. Ouellette, H. Xu, M. Bourgoin, and E. Bodenschatz, "An experimental study of turbulent relative dispersion models," New J. Phys. **8**, 109 (2006).

[42] T. Burghelea, E. Segre, I. Bar-Joseph, A. Groisman, and V. Steinberg, "Chaotic flow and efficient mixing in a microchannel with a polymer solution," Phys. Rev. E **69**, 066305 (2004).

[43] T. Watanabe and T. Gotoh, "Coil-stretch transition in an ensemble of polymers in isotropic turbulence," Phys. Rev. E **81**, 066301 (2010).

[44] A. Robert, T. Vaithianathan, L. R. Collins, and J. G. Brasseur, "Polymer-laden homogeneous shear-driven turbulent flow: a model for polymer drag reduction," J. Fluid Mech. **657**, 189–226 (2010).